Research Square

Preprints are preliminary reports that have not undergone peer review.
They should not be considered conclusive, used to inform clinical practice,
or referenced by the media as validated information.

High-performance Ni–Gd@BTC MOF electrodes enable enhanced Energy storage in aqueous asymmetric supercapacitors

Aishwarya Senrayalraj
PSG College of Arts and Science
Yogalakshmi Vadivelu
PSG College of Arts and Science
Srither S.R.
Koneru Lakshmaiah Education Foundation
Ramachandran Balaji
Koneru Lakshmaiah Education Foundation
Rajkumar Muniyandi
PSG College of Arts and Science
Balakumar Muniandi
bmuniandi@uidaho.edu

University of Idaho

Article

Keywords:

Posted Date: March 3rd, 2026

DOI: https://doi.org/10.21203/rs.3.rs-8709590/v1

License: This work is licensed under a Creative Commons Attribution 4.0 International License.
Read Full License

Additional Declarations: No competing interests reported.

High-performance Ni–Gd@BTC MOF electrodes enable enhanced

Energy storage in aqueous asymmetric supercapacitors

Aishwarya Senrayalraj[1], Vadivelu Yogalakshmi[1], S.R.Srither[2], Ramachandran Balaji[2], Muniyandi Rajkumar[1*], Muniandi Balakumar[3*]

[1]Department of Chemistry, PSG College of Arts and Science, Coimbatore 641014, India.

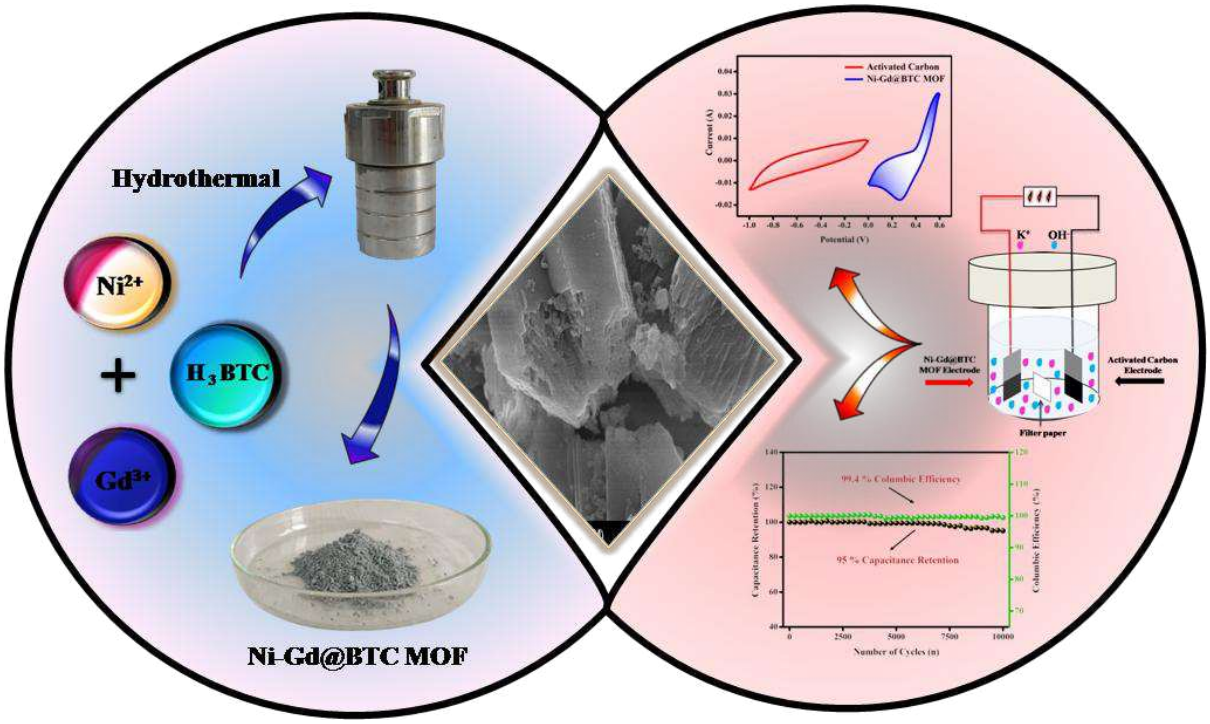
[2]Department of Electronics and Communication Engineering, Koneru Lakshmaiah Education Foundation, Vaddeswaram, Andhra Pradesh 522302, India

[3] Department of Electrical and Computer Engineering, University of Idaho, Moscow, Idaho, USA, 83844

[*]Corresponding author e-mail:*rajkumar.m@psgcas.ac.in*

[*]Corresponding author e-mail:*bmuniandi@uidaho.edu*

Graphical Abstract



Abstract

Metal–organic frameworks (MOFs) have emerged as promising electrode materials for next-generation supercapacitors owing to their high density of redox-active sites and tunable architectures. Here, we report the hydrothermal synthesis of a bimetallic Ni–Gd@BTC MOF and evaluate its electrochemical energy-storage performance. The resulting material exhibits a layered, sheet- like morphology that promotes rapid ion transport and efficient charge-transfer kinetics. When employed as an electrode in a three-electrode configuration, Ni–Gd@BTC delivers a high specific capacitance of 910.98 F g^{-1} at 0.7 A g^{-1}, underscoring its strong charge-storage capability. The electrode also demonstrates excellent long-term durability, retaining 88% of its initial capacitance with 98% Coulombic efficiency after 10,000 charge–discharge cycles at 5 A g^{-1}. To assess device-level performance, we assembled a battery-type asymmetric supercapacitor (Ni–Gd@BTC MOF//AC). The device achieves an energy density of 43.11 Wh kg^{-1} and a power density of 3200 W kg^{-1} at 1 A g^{-1}, along with 90 % capacitance retention after 10,000 cycles at 5 A g^{-1}. Collectively, these results establish Ni–Gd@BTC MOF as a highly effective electrode material with substantial potential for high-performance electrochemical energy-storage systems.

1. Introduction

The accelerating global transition toward renewable energy has intensified the demand for efficient and high-performance energy-storage technologies. Supercapacitors have emerged as strong candidates for next-generation storage systems capable of complementing intermittent renewable power sources, owing to their high power density, long cycling life, and rapid charge–discharge characteristics[1,2].While supercapacitors excel at delivering high power density [3], conventional batteries offer superior energy density[4]. To combine the advantages of both technologies, considerable research has focused on developing hybrid or asymmetric supercapacitor configurations that bridge this performance gap[5].Central to this effort is the design of electrode materials that can achieve high energy density without compromising cycling stability or rate capability.

Metal–organic frameworks (MOFs) have attracted significant attention as electrode materials for advanced supercapacitors due to their tunable architectures, diverse topologies, and abundance of redox-active metal centers that enhance charge-storage behavior. However, monometallic MOFs often exhibit limited electrochemical performance arising from their restricted number of active sites and inherently low electrical conductivity. These constraints lead to reduced capacitance, energy density, and power density, ultimately limiting their practical applicability in high-performance supercapacitors systems [6,7].

To address these challenges, several strategies have been developed to enhance the electrochemical performance of metal–organic frameworks (MOFs)[8,9].Recent efforts have focused on tailoring their structure, morphology, and composition to improve electrical conductivity, facilitate ion transport, and strengthen overall stability. Among these approaches, the construction of bimetallic MOFs by incorporating a secondary metal ion has emerged as particularly effective[10]. This strategy significantly enhances conductivity,

increases the density of redox-active sites, and reinforces structural integrity. The synergistic interaction between two metal centers enables multiple redox processes, thereby improving charge-transfer pathways and accelerating electrochemical kinetics. As a result, bimetallic MOFs often exhibit higher specific capacitance, energy density, and power density compared to their monometallic analogues[11].While transition-metal–based bimetallic MOFs provide improved activity, their conductivity and long-term cycling stability can still be limited. Introducing 4f rare-earth metals offers a promising solution to these issues[12,13]**.**The unique electronic configurations of rare-earth ions can modulate the coordination environment and expand the pore structure, creating larger cavities and more accessible active sites for electrolyte ions[14]. Consequently, rare-earth incorporation effectively tunes the electronic structure of transition-metal MOFs, generates a greater number of electroactive centers, and markedly enhances their electrochemical performance[15].

Among transition-metal-based frameworks, nickel metal–organic frameworks (Ni-MOFs) have attracted substantial interest for supercapacitor applications due to their favorable electrochemical properties and structural tunability. Unlike purely electric double-layer materials, Ni-based systems exhibit pronounced pseudocapacitive behavior arising from the highly reversible Ni^{2+}/Ni^{3+} redox couple, which enables efficient faradaic charge storage. The robust redox activity of Ni ions supports rapid charge–discharge kinetics and contributes to the high energy density and cycling stability commonly observed in Ni-MOF electrodes [16–18]. Incorporating gadolinium—a rare-earth lanthanide with partially filled 4f orbitals—further enhances the electrochemical response by introducing additional redox-active centers and improving electronic conductivity. Gd ions can increase the dielectric constant and induce lattice distortions or oxygen vacancies within the MOF framework, thereby facilitating ion diffusion and boosting overall charge-storage capability[19,20]. Moreover, the

synergistic interaction between Ni and Gd in a bimetallic structure strengthens the framework and mitigates structural degradation, ultimately improving long-term cycling durability.

In this study, we synthesized a novel Ni–Gd@BTC metal–organic framework(MOF) and employed it as a high-performance electrode material for hybridsupercapacitor applications. The material was prepared via a simple and scalablehydrothermal route, offering a cost-effective strategy for fabricating advancedelectroactive frameworks. The synergistic integration of nickel (Ni^{2+}/Ni^{3+}) andgadolinium (Gd^{3+}) metal centers with trimesic acid (H_3BTC) ligands markedlyimproves the electrochemical characteristics of the MOF by providing abundantand accessible redox-active sites. The incorporation of Gd^{3+} not only enhanceselectrical conductivity but also strengthens the structural stability of theframework.The resulting Ni–Gd@BTC exhibits a morphology that supports efficientelectrolyte-ion diffusion and rapid charge transfer—features essential forachieving high energy and power densities. When used as an electrode, thematerial delivers a remarkable specific capacitance of 910.98 F g^{-1} at 0.7 A g^{-1},demonstrating excellent charge-storage capability. It also maintains 90.6%capacitance retention after 10,000 charge–discharge cycles, underscoring itsoutstanding stability and reversibility. Collectively, these results highlightNi–Gd@BTC as a highly promising candidate for next-generation, high-performance supercapacitor systems, combining superior electrochemicalactivity with exceptional durability.

2. Material and Methods

2.1. Chemicals/Reagents

Nickel(II) Chloride Hexahydrate ($NiCl_2.6H_2O$), Gadolinium(III) Chloride Hexahydrate ($GdCl_3.6H_2O$), TrimesicAcid (H_3BTC) and Dimethyl Formamide (DMF) were purchased from Sigma Aldrich Co., Ltd. were used without any further purification. The Conductivity carbon (Super P), Polyvinylidene Fluoride (PVDF) *N*-Methyl Pyrrolidinone (NMP) were obtained from Research Supporters India., were used received. Deionized water is used as the source for performing all the experiments.

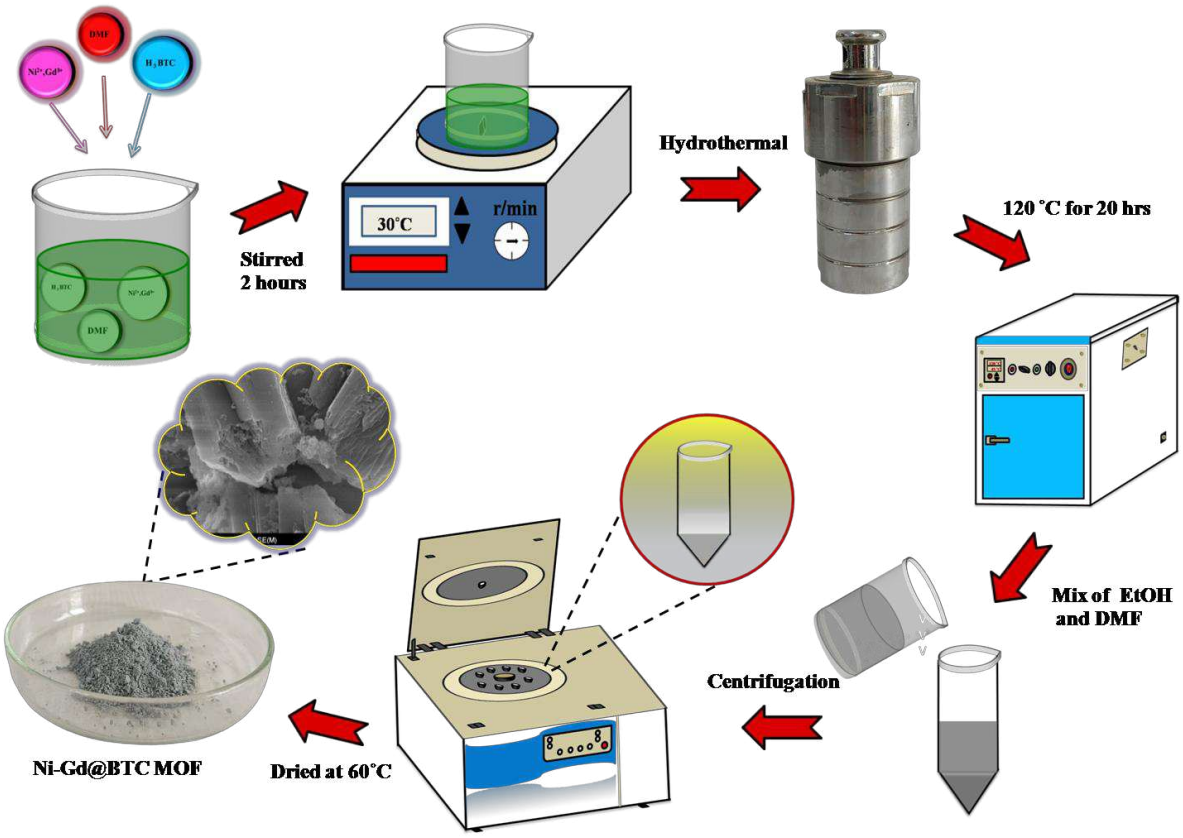
2.2. Experimental procedure for the synthesis of Ni-Gd@BTC MOF

Ni-Gd@BTC MOF was synthesized by a typical hydrothermal reaction. 1mmol of $GdCl_3.6H_2O$, 2 mmol of $NiCl_2.6H_2O$ and 4 mmol of Trimesic Acid were dissolved in 30 mL of Dimethyl Formamide and stirred vigorously for 2 hours. Then the mixed solution was transferred to a 50 mL Teflon-lined autoclave for the hydrothermal treatment at 120˚C for 20 hours. After being cooled to room temperature, the resultant grey colored precipitate were separated from the reaction mixture, by centrifugation and washed thoroughly with DMF and ethanol mixture to un-reacted starting materials (as shown in scheme. 1). Finally obtained solid was dried at a vacuum oven at 60˚C for an entire night for further analysis.

2.3. Measurements and general methods

Powder X-ray diffraction measurements were carried out using D2 Phaser, Bruker AXS Inc) was utilized to determine the crystal structure of the Ni-Gd@BTC MOF. Raman spectra of synthesized Ni-Gd@BTC MOF material were obtained from a confocal Raman Spectroscopy with an incident monochromatic light as a lased source. The surface morphology of synthesized material was observed using FE-SEM (SEM, JSM-IT200, JEOL

Ltd), with elemental distribution usingEnergy Dispersive Spectroscopy (EDS, JSM-IT200, JEOL Ltd.).In order to further evaluate the material's elemental composition X-ray Photoelectron Spectroscopy (XPS,PHI 5000 Versa Probe III, ULVAC-PHI, Inc.) were employed. Electrochemical measurements were performed with the aid of electrochemical workstation (OrigolysElectrochem equipped with Origo master 5 software).



Scheme.1 ***Synthesis of*** **Ni-Gd@BTC** ***MOF***

2.4. Electrode preparation and electrochemical evaluation

The synthesized Ni-Gd@BTC MOF (as active material), Activated carbon (as a conductivity carbon) and Polyvinylidene Fluoride (as binding agent) in stiochiometricat mass ratio 8:1:1 were grounded using a mortar and pestle for 30 minutes; *N*-Methyl Pyrrolidinone

(NMP) was added to this mixture and stirred vigorously to make a homogeneous slurry. Prior to the electrode fabrication, commercially available, Graphite Sheet (GS 1 × 2cm) substrate was ultrasonically cleaned with ethanol for 15 minute. Finally the homogeneous slurry was uniformly coated on 1 × 2 cm was evenly covered with the resultant slurry, which had an effective area of 1 cm^2 substrate and dried in a vacuum oven at 60˚C for overnight. The recorded mass of Ni-Gd@BTC MOF loaded is approximately 2 mg. All the electrochemical tests were performed at room temperature using, 1 M KOH electrolyte in a standard three electrode cell configuration. Thus, Ni-Gd@BTC MOF coated on GS, Ag/AgCl, Pt wire serves as working, reference and counter electrodes respectively. Cyclic Voltammetry and Galvanstatic Charge/Discharge (GCD) measurements were recorded to determine the capacitance of the active material. The stability tests of theNi-Gd@BTC MOF electrode material was performed over 10,000 cycles by applying constant current density of 5A/g. An Electrochemical Impedance Spectroscopy (EIS) study was carried out at a frequency ranges from 1 M Hz to 100m Hz. Furthermore an asymmetric supercapacitor (ASC) hybrid assembled by employing Ni-Gd@BTC MOF as positive electrode along with activated carbon as negative electrode in 1M KOH electrolytic solution.

3. Results and Discussion

3.1. FE-SEM and EDX analysis

The surface morphology of the synthesized Ni–Gd@BTC MOF was examined using scanning electron microscopy at different magnifications as shown in Fig. (a–d),. Figure.1 (a) shows well-defined rod-like microcrystal with smooth surfaces, which show that the metal ions ($Ni^{2+/3+}$ and Gd^{3+}) and BTC organic linkers work together well and grow uniformly. Effective control over nucleation and growth during synthesis is suggested by the rods' uniform distribution and high aspect ratio [21]. Figure.1 (b) shows how the rod-like

components come together to form a rod-like arrangement that creates a three-dimensional network of connections. For supercapacitor applications, such a hierarchical shape is beneficial because it promotes electrolyte ion diffusion. The rods show rough and porous surfaces with irregular edges, as shown in Figure.1 (c). These pores can significantly enhance ion transportation and provide active channels for charge storage. The presence of fine particles and surface roughness attributed to Gd^{3+} incorporation as shown in Figure.1 (d), which introduces structural distortion and surface defects. These modifications lead to an increased number of electro-active sites and improved electrical conductivity. To verify the elemental composition and chemical distribution, Energy Dispersive X-ray (EDX) analysis combined with elemental mapping was conducted, as shown in Figure.1 (e-j) The synthesized rod-like hierarchical porous morphology of Ni–Gd@BTC MOF offers an ideal structure for supercapacitor electrodes by providing high porosity, short ion diffusion paths, and abundant redox-active centers for enhanced peseudocapacitivecapacitive performance.

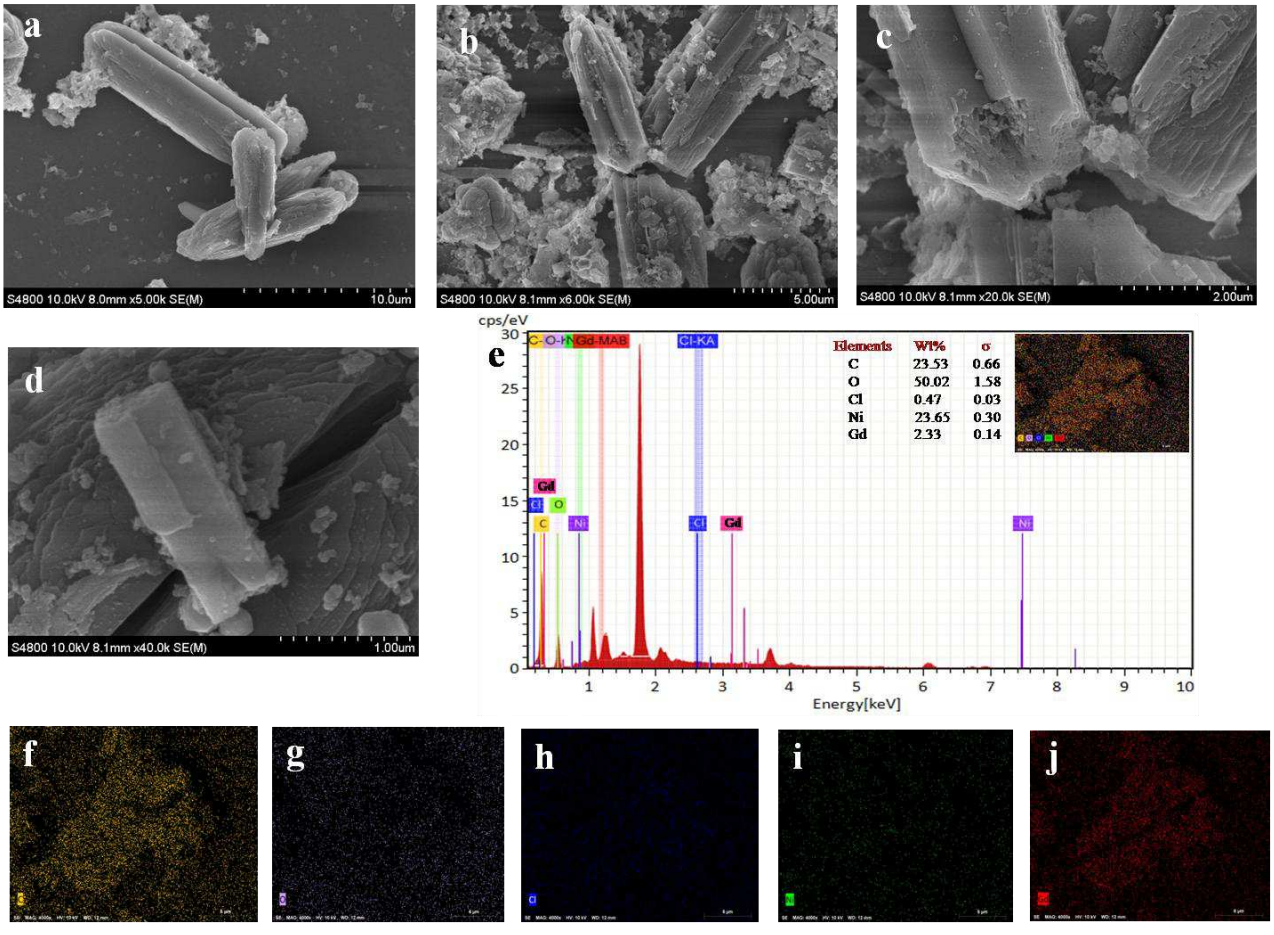


Figure.1 (a-d) FESEM images of synthesized Ni-Gd@BTC bimetallic MOF at different magnifications; (e-j) EDX images of Co-Gd@BTC MOF.

3.2. Powder X-ray diffraction and Raman measurements

The X-ray diffraction (XRD) pattern of the produced Ni–Gd@BTC metal–organic framework (MOF) is shown in the Figure.2 (a). The diffraction peaks observed in the 2θ range of 5°–60° confirm that the material is crystalline. Previous research indicates that the characteristic reflections at 2θ ≈ 9°, 12°, 14°, 15°, 16°, 20°, and 25° correspond to the typical diffraction peaks of the parent Ni–BTC framework[22]. The successful synthesis of the bimetallic Ni–Gd@BTC MOF is validated by the retention of these peaks (2θ ≈ 31°, 35°, 40°, 44°, and 52°) after incorporating gadolinium ions[23]. This suggests that the structure based on benzene-1,3,5-tricarboxylate (BTC) remains intact. Additionally, the absence of any additional peaks associated with gadolinium oxide or hydroxide phases indicates high phase purity and the full integration of Gd ions into the Ni–BTC lattice, rather than the formation of a separate crystalline phase. The substitution of Gd^{3+} ions, which have a larger ionic radius than Ni^{2+}, may have induced some lattice strain or distortion. Consequently, this could result in slight changes in peak positions and minor broadening compared to the Ni–BTC pattern. Overall, the produced Ni–Gd@BTC MOF exhibits good crystallinity, as evidenced by the distinct and sharp peaks.

The successful creation of the framework is indicated by the multiple distinct peaks in the range of 250 to 1250 cm^{-1} in the Raman spectra of the synthesized Ni–Gd@BTC MOF display seen in Figure 2 (b). The M–O stretching vibrations are responsible for the conspicuous bands at 580 cm-1 and 660 cm-1, which correspond to the coordinated Ni–O and Gd–O bonds.This demonstrates strong metal–ligand interactions within the MOF structure. The peak observed at 750 $cm^{-1}$is associated with the O–C–O symmetric stretching vibration

of the carboxylate group, confirming the coordination of the organic linker to the metal centers.Additionally, the bands at 830 cm^{-1} and 890 cm^{-1} are linked to the C–H bending and aromatic ring deformation modes of the organic linker. The band at 1180 cm^{-1} arises from C–C stretching vibrations within the aromatic ring.[24,25] The presence of these characteristic peaks confirms the retention of the organic framework and the successful incorporation of both Ni and Gd ions. The coexistence of dual metal centers enhances structural stability, electron density, and charge transfer efficiency, all of which are essential for improving the performance of electrochemical energy storage.

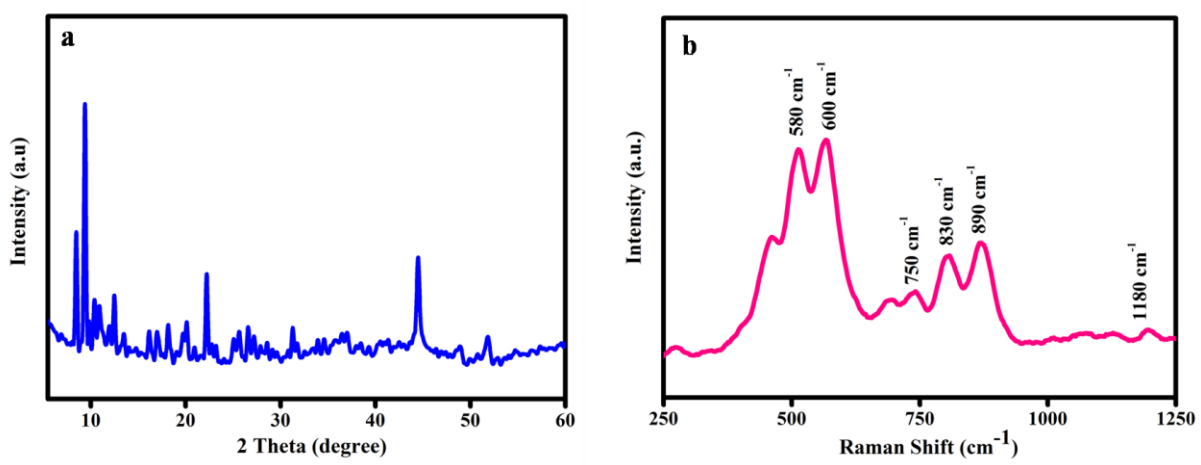


Figure.2(a) XRD graph and (b) Raman shits of Ni-Gd@BTC MOF

3.3. X-ray photoelectron spectroscopy

The X-ray Photoelectron Spectroscopy (XPS) analysis provides detailed insights into the elemental composition and chemical states present in the Ni-Gd@BTC MOF. The survey spectrum of Ni-Gd@BTC MOF as depicted in Figure.3 (a)reveals predominant peaks corresponding to Nickel, Gadolinium, Chlorine, Carbon and Oxygen verifying the incorporation of both metal ions within the organic framework. The high-resolution Ni2p

spectrum exhibits distinct Ni $2p_{3/2}$ and Ni $2p_{1/2}$ peaks along with characteristic satellite features as depicted Figure.3 (b) Which collectively indicate the coexistence of Ni^{2+} and Ni^{3+} species at the binding energy of 856 eV and 875 eV. This mixed-valence behavior is beneficial for supercapacitor electrodes because it enhances Faradic redox reactions, contributing to improved pseudocapacitive performance[26].Figure.3 (c) Shows the Gd 4d spectrum confirms the presence of Gadolinium ion in the structure, displaying distinct peaks for Gd $4d_{5/2}$ and Gd $4d_{3/2}$ at the binding energies 145.2 eV and 152 eV[27].The presence of Gadolinium ion enhances electron mobility, stabilize the framework and introduce additional redox-active sites. These factors collectively contribute to improved conductivity and long-term cycling stability. The presence of residual chloride species, originating from the metal precursors, is evident from the distinctive Cl $2p_{3/2}$ and Cl $2p_{1/2}$ peaks observed at binding energies of 198 eV and 200 eV in the high-resolution Cl 2p spectra as depicted in Figure.3 (d) These Cl^- ions may remain loosely associated with the metal centers, which can affect electrical conductivity and enhance charge transfer.The high-resolution C 1s spectra show distinct peaks at the binding energies of 284.6 eV, 286 eV and 288.5 eVcorresponding to aromatic C-C bonds, C-OH groupand carboxylate HO-C=O species as shown in Figure.3 (e) These functional groups indicate that the MOF framework possesses a high surface area and structural stability, confirming the effective coordination of the organic ligand with Nickel and Gadolinium metalions. The O 1s spectra confirm the presence of coordinated metal–oxygen bonds and organic oxygen functionalities as depicted in Figure.3 (f) The spectra display peaks corresponding to O–H, Ni/Gd–O and C–O–C bonds which show the distinctive peaks at 530.5 eV, 531.7 eV and 532.3 eV respectively[28]. The strong coordination of Ni/Gd–O establishes redox-active centers that are essential for improved pseudocapacitive behavior in supercapacitor applications

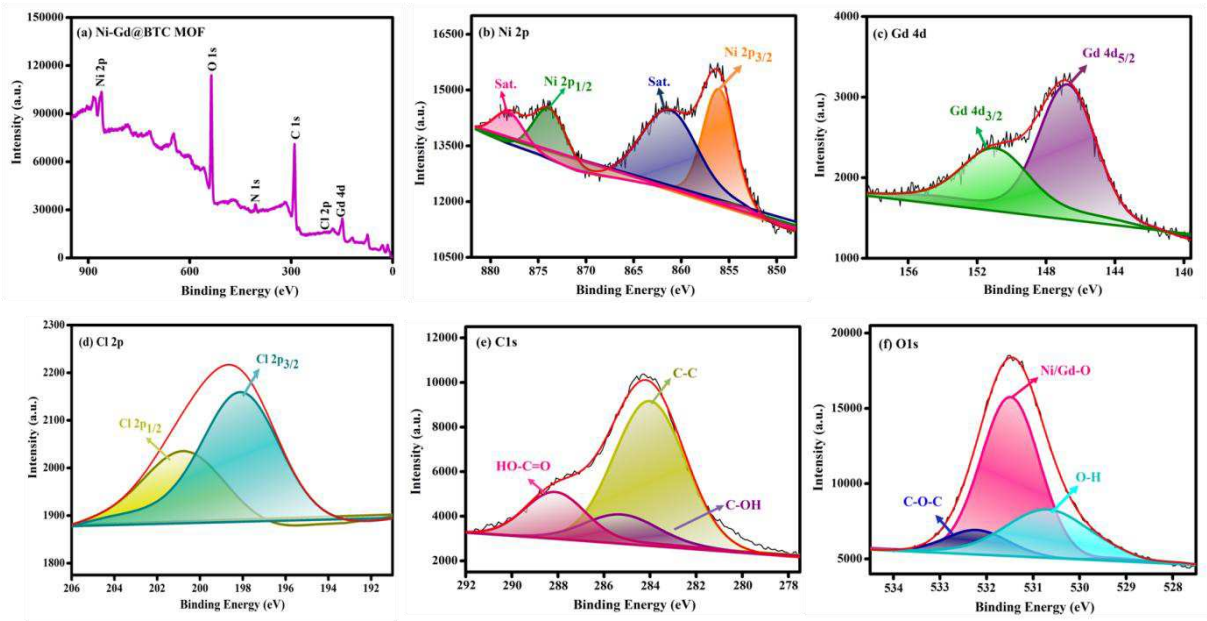


Figure. 3XPS spectrum of Ni-Gd@BTC MOF (a) Full range survey; (b) Ni 2p; (C) Gd 4d; (d) Cl 2p; (e) C 1s; (f) O 1s.

3.4. Electrochemical Measurements

The electrochemical performance of the Ni-Gd@BTC MOF electrode materials was evaluated using cyclic voltammetry, galvanostatic charge/discharge, and electrochemical impedance spectroscopy techniques. The voltammetric curves show how well the electrode works at different scan rates in a voltage range of 0 to 0.5 V. Figure.4(a) shows the results of cyclic voltammetry (CV) measurements at scan rates of 3, 5, 10, 20, 30, 40, and 50 mV/s, from 0 to 0.5 V.The current responses and the area under the CV curve of Ni-Gd@BTC reveal redox peaks, indicating the redox reactions occurring on the electrode surface. The CV scans should be symmetrical since non-faradic capacitance is not affected by scan rate or potential. But the asymmetrical shape and rate-dependent behavior of the CV scans point to faradic reactions, which are the typical characteristics of pseudo-capacitive type material [29,30]. The possible electrochemical reactions at the interface between the electrode and electrolyte are as follows;

$$NiO + OH^- + H_2O \leftrightarrow Ni(OH)_2$$

$$Ni(OH)_2 + OH^- \leftrightarrow NiOOH + H_2O + e^-$$

$$Gd^{3+} + 3OH^- \leftrightarrow Gd(OH)_3$$

In alkaline medium the faradic behavior of Ni-Gd@BTC MOF is mainly governed by the reversibility of $Ni^{2+/3+}$ redox transition while Gd enhances the structural stability and ionic conductivity, improved ionic diffusion and stabilization of MOF lattice, The synergistic interactions between $Ni^{2+/3+}$ or Gd^{3+} centers thus enhance electrochemical activity, structural robustness and cycling stability[19,31,32]. The most significant redox peaks in a slow scan rate were found at an anodic potential of 0.43 V and a cathodic potential of 0.36 V. As a result, the current value of the peaks increased as the scan rate increased.This signifies that at high scan rates, in a less time interval gives ionic intercalation at the electrode surface.

To better understand the charge storage process, a power law was utilized to determine if the storage happens through diffusive or capacitive mechanisms in order to have a better understanding of the charge storage process. This is represented as,

$$\mathbf{i = av^b} \qquad (\mathbf{1})$$

$$\mathbf{\log(i) = \log(a) + b \log(v)} \qquad (\mathbf{2})$$

Wherei was a peak current, v was the scan rate, a and b were adjustable parameters.A typical b value of 1 suggests capacitive-controlled charge storage mechanism, while below 0.5 suggests complete diffusive-controlled charge storage mechanism as depicted in Figure.4 (b), the calculated b-value for Ni-Gd@BTC MOF electrode are 0.54 for the redox process. These results demonstrate that the diffusive mechanism and partial capacitive mechanism were the main factors influencing the electrochemical storage kinetics of electrode material.

Additionally, the percentage contribution of electrode material at different scan speeds is shown in the equation below,

$$\mathbf{i(v) = k_1 v + k_2 v^{1/2}} \qquad \mathbf{(3)}$$

Thus, k_1v and $k_2v^{1/2}$ reflect the capacitive and diffusive contributions, where v is the scan rate, k_1 and k_2 were constants, and i is the peak current. [33,34].At a scan rate of 3 mV/s, the capacitive contribution was 23.2% (Figure 4(c)). This percentage increased to 55.2% when the scan rate was raised to 10 mV/s (refer to Figure 4(d)). However, as the scan rate increased from 5 to 50 mV/s, the proportion of both diffusive and capacitive contributions during the oxidation and reduction process at the working electrode in a 1 M KOH electrolyte as illustrated in Figure 4(e).

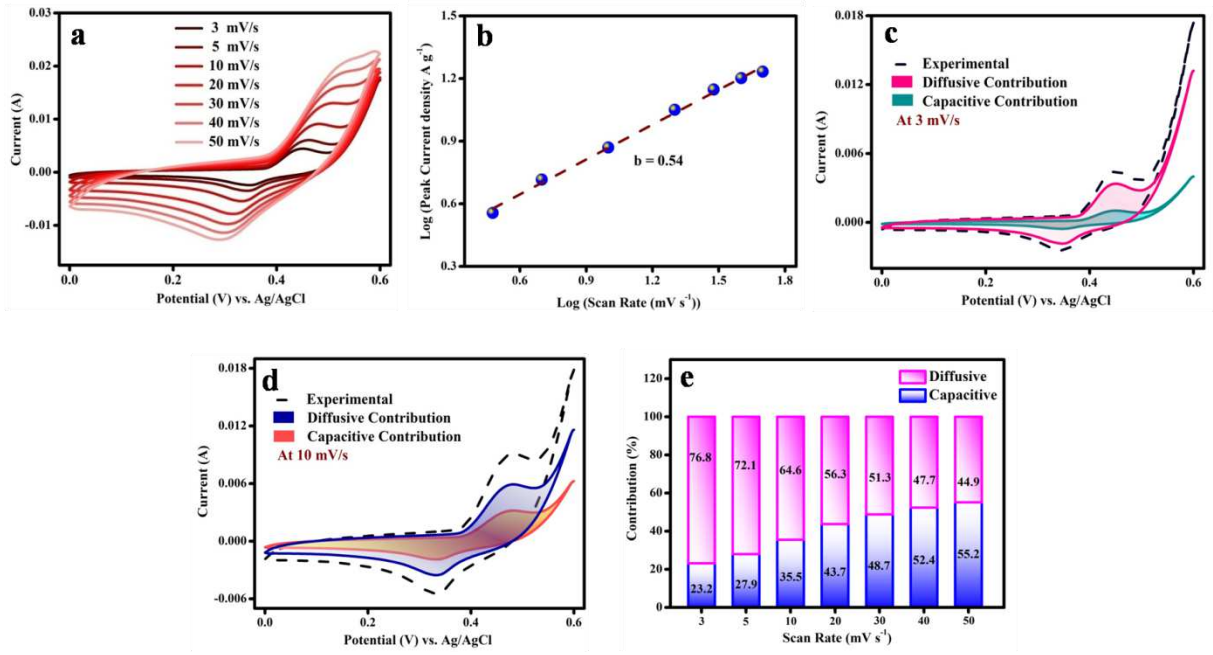


Figure. 4 (a) Cyclic voltammetry(CV) curves of Ni-Gd@BTCat different scan rates; (b)The plot between the log of scan rate and log of peak current density; (c,d) Capacitive and diffusive contribution of Ni-Gd@BTC MOF at scan rate of 3 mV/s and 10 mV/s ; (e) Bar graph Capacitive and Diffusive contribution at different scan rates in 1M KOH electrolyte with increasing scan rate.

Furthermore, Figure 5(a) displays the Ni-Gd@BTC MOF's charging and discharging curves at various current densities within a constant potential window of 0 to 0.5 V.The MOF electrode exhibits galvanostatic charge-discharge (GCD) profiles that align well with their cyclic voltammetry (CV) profiles. To calculate the specific capacitance the following formula was utilized,

$$\boldsymbol{Cs = \frac{I \times \Delta t}{m \times \Delta V}} \qquad (4)$$

Here "I" represents the applied current, "Δt" denotes the discharge time, "m" refers to the mass loading of active material in grams against the graphite sheet electrode, and "V" signifies the potential window. The variables "Cs" and "ΔV" indicate specific capacitance and voltage window, measured in farads per gram (Fg^{-1}) and volts (V), respectively. Additionally, "Δt" stands for discharge time in seconds, while "t_D" and "t_C" represent the discharge and charge times obtained from the galvanostatic charge-discharge (GCD) curve. The GCD curves display non-linear characteristics with a clear plateau region that signifies the pseudocapacitive-type behavior. The specific capacitance of the MOF electrode material was calculated to be 910.98 F g^{-1} (at 0.7 A g^{-1}), 793.44 F g^{-1} (at 0.9 A g^{-1}),681.43 F g^{-1} (at 1 A g^{-1}), 594.82F g^{-1} (at 2 A g^{-1}), 473.40 F g^{-1} (at 3 A g^{-1}), 378.45F g^{-1} (at 4 A g^{-1}), 272.02 F g^{-1} (at 5 A g^{-1}) as shown in Figure.5 (b). Thus, on increasing the current density, the specific capacitance of the electrode material decreases due to the attribution of slower electrochemical activities caused by limited ion penetration into the inner pores at higher current densities [35]. The specific capacitance of higher than other reported works that are compared in Table.1

An EIS analysis was conducted in order to assess the charge transfer phenomenon using the frequency concept. The Rs and Rct values were found to be 2.35 Ω and 0.78 Ω, respectively, when the Ni-Gd@BTC MOF was taken into consideration, as can be seen in

Figure 5 (c).These indicates that the material has good ionic conductivity and minimal ohmic resistance. The warburg impedance (79.13 mS)in the form of extended lines with angles 40˚ to 50˚ as inserted in Figure.6(c)) indicating that the fabricated Ni-Gd@BTC MOF electrode material has low charge transfer resistance, which makes the fabricated electrode is more conductive. The combined interfacial capacitance (C_{dI}) was noted to be 89.40 mF. This reveals the fabricated material has lower solution resistance and quicker ionic diffusion mechanism to store charge more than others. The cyclic capabilities were examined through galavnostatic charge/discharge test was performed at a current density of 5 A/g with the potential range of 0 to 0.5 V. Notably, after 10,000 cycles the retention capacitance of 88% with a 12 % loss from its initial retention. Whenever there is a loss of active material causes decreases in capacitance as the number of cycles raised in a KOH solution. Additionally, a columbic efficiency of 98% was attained, indicating minimal internal resistance and good ion reversibility throughout each cycle of electrochemical reactions as shown in Figure 5 (d).The obtained better electrochemical performance suggests that the Ni-Gd@BTC MOF can work as suitable candidate for supercapacitor application and their measurements were compared with previously reported data as given in Table.1.

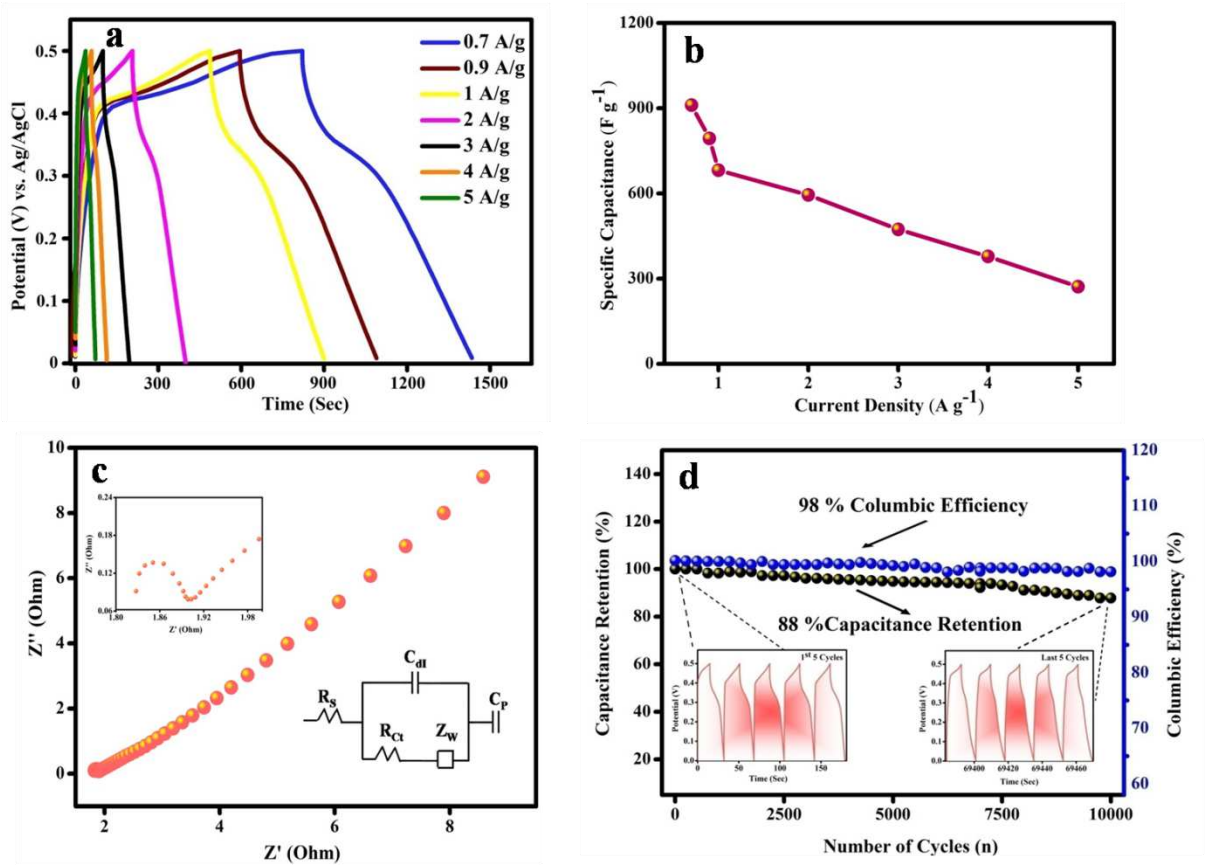


Figure. 5 (a) The Charge Discharge curves of Ni-Gd@BTCMOFat various current densities;(b) Specific capacitance Vs current density for Ni-Gd@BTCMOF (c) EIS spectrum of Ni-Gd@BTCMOF(inserted equivalent circuit); (d) cycling stability of the Ni-Gd@BTCMOF supercapacitor

Table 1. Comparison of prepared Ni-Gd@BTC MOF electrode with various previously reported data for Charge Discharge measurements

Material	Morphology	Electrolyte	Specific Capacitance	Capacitance Retention	Reference
Ni MOF	Flower like spheres at nanosheets	6 M KOH	920 F g^{-1} at 1 A g^{-1}	61 % after 3,000 cycles	[36]
Ni MOF/MWCNTs	Aggregated nanosheets	6 M KOH	900 F g^{-1} at 0.5 A g^{-1}	82 % after 1,000 cycles	[37]
Ni-Mn MOF	Nanosheets	2 M KOH	447.5 F g^{-1} at 0.5 A g^{-1}	65.3 % after 10,000 cycles	[38]
V_2O_5/Ni MOF	Petal like nanosheets	3 M KOH	546 F g^{-1} at 1 A g^{-1}	10,000 cycles	[39]
La doped Ni MOF	Flower like cross-linked nanosheets	2 M KOH	159.9 mA h/g	-	[40]
Cr doped Ni MOF	3D nanosheets	3 M KOH	853 F g^{-1} at 1 A g^{-1}	64.48 % after 5,000 cycles	[41]
Ni-Co MOF @rGO	Spherical particles	6 M KOH	860 F g^{-1} at 1 A g^{-1}	-	[42]
LONH composites	Triangle nanosheets	3 M KOH	783 F g^{-1} at 1 A g^{-1}	78.7% at 5 A g-1	[43]

Ni-Gd@BTC MOF	**rod-likestructure**	**1 M KOH**	**910.98 F g^{-1} at 0.7 A g^{-1}**	**88% after 10,000 cycles**	**This work**

3.5. Asymmetric Battery type Supercapacitor cell assembly

An Asymmetric Supercapacitor (ASC) assembly (see Figure 6(a)) was developed to showcase the practical application of the Ni-Gd@BTC Metal-Organic Framework (MOF). In this setup, activated carbon serves as the negative electrode, while the Ni-Gd@BTC MOF functions as the positive electrode. The two electrodes are then separated by filter paper, which acts as a separator to maintain physical distance between them during ionic conduction, thereby preventing short circuits. Before testing the ASC device, both positive and negative electrodes were electrochemically activated separately in a three electrode cell assembly, using different potential window; 0-0.5 V for Ni-Gd@BTC MOF and -0.1 – 0 V for Activated Carbon (AC) as illustrated in Figure.6 (b).

Furthermore, to ensure a balanced mass loading between the positive and negative electrodes, the following equation is utilized;

$$\frac{\boldsymbol{m^-}}{\boldsymbol{m^-}} = \frac{\boldsymbol{c_-} \times \boldsymbol{\Delta v_-}}{\boldsymbol{c_+} \times \boldsymbol{\Delta v_+}} \quad (\mathbf{6})$$

Here “m” stands for mass, c means specific capacitance and “v” potential window of positive and negative electrodes, respectively. The cyclic voltammograms of Ni-Gd@BTC MOF//AC ASC hybrid battery type device were recorded at the potential window of 0-1.6 V by increasing the scan rates (5, 10, 20,30,40,50 mV/s) indicates the charge storage reversibility of ASC device which shows the hybrid nature of the electrode material as shown in Figure.6 (c)

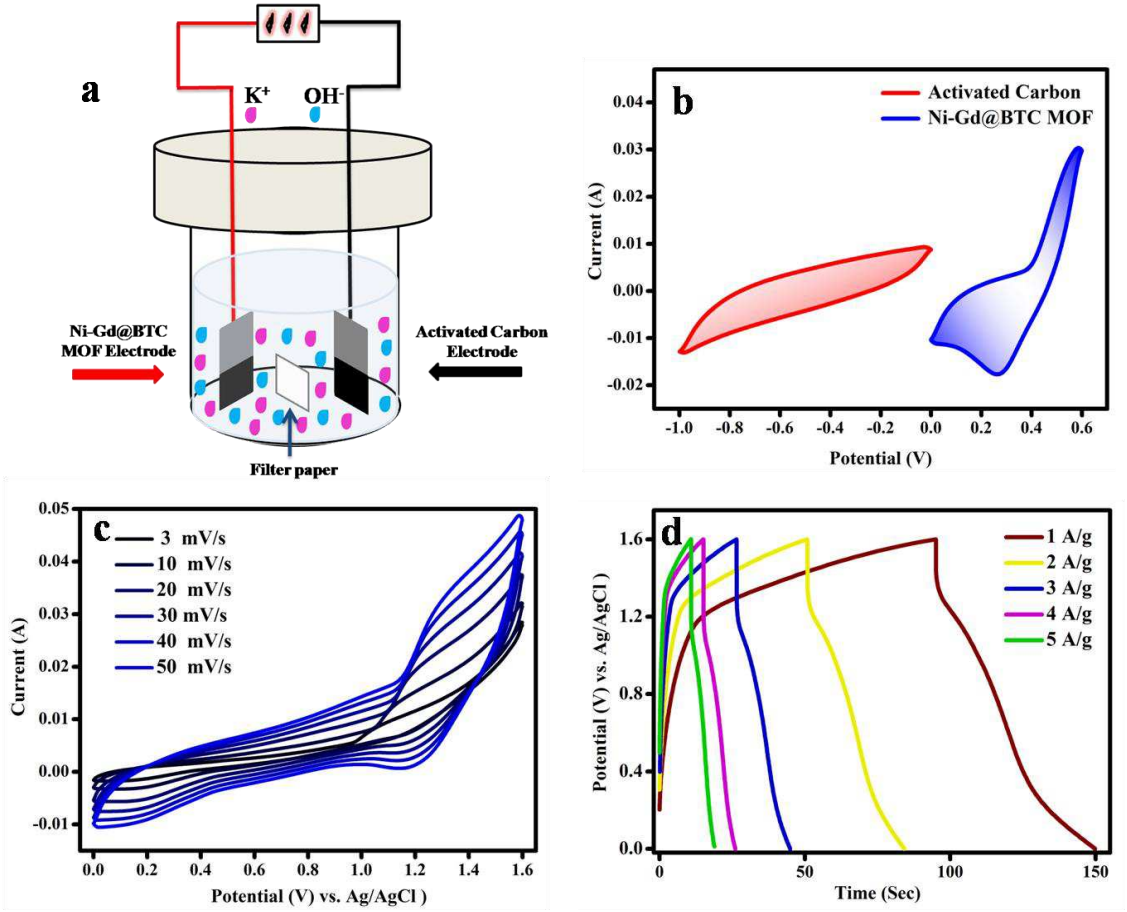


Figure. 6 (a) Ni-Gd@BTC MOF//AC assembly; (b) Cyclic Voltammetry(CV) curves of Activated carbon and Ni-Gd@BTC MOF//AC at 100 mV/s; (c) CV curves of Ni-Gd@BTCat different scan rates; (d) GCD curves of Ni-Gd@BTC MOF//ACat various current densities;

The GCD curves of Ni-Gd@BTC MOF//AC were formed with an operating potential window of 0-1.6 V demonstrating the non-linear behavior of GCD Curves with different current densities (1, 2, 3, 4 and 5 A/g) and affirmed the hybrid characteristics of the device as shown at in Figure.6 (d). The energy density (E_D), power density (P_D) and columbic efficiency calculations[44] are calculated from specific capacitance (C_s), potential (V), Charging (t_C) and discharging time (t_D) using the following formulas,

$$E_D = \frac{1}{7.2} C_{ASC} (\Delta V)^2 \quad (7)$$

$$P_D = \frac{E_D \times 3600}{\Delta t} \quad (8)$$

$$\eta_t = \frac{t_D}{t_C} \times 100 \quad (9)$$

The value of the specific capacitance also calculated as 121.25 F/g at 1 A/g which decreased with increasing the current densities as depicted in Figure.7 (a). The maximum energy density and power density of 43.11 Wh/kg and 3200 w/kg was given by the device at current density of 1 A/g was as shown in Figure.7 (b). EIS was also performed to test the conductivity of the hybrid assembly as depicted in Figure.7 (c). The value of R_s was 0.132 indicating the good ionic conductance and electron-transfer at the electrode-electrolytic interfaces, the Warburg and combined interfacial capacitance (C_{dl}) exhibited as 72.36 mS and 143.267 mF. After 10,000 cycles of charging and discharging in a 1M KOH solution at a current density of 5 A/g, the ASC Ni-Gd@BTC MOF//AC device demonstrated a capacitance retention of 90% and a coulombic efficiency of 99.1%. As illustrated in Figure 7(d), this high level of stability highlights the impressive endurance of the active electrode material under prolonged cycling conditions. The ASC Ni-Gd@BTC MOF//AC cell assembly shows, very low resistance, excellent retention capability and holds good for high-rate capacitive behavior with a notable pseudo-capacitive component.

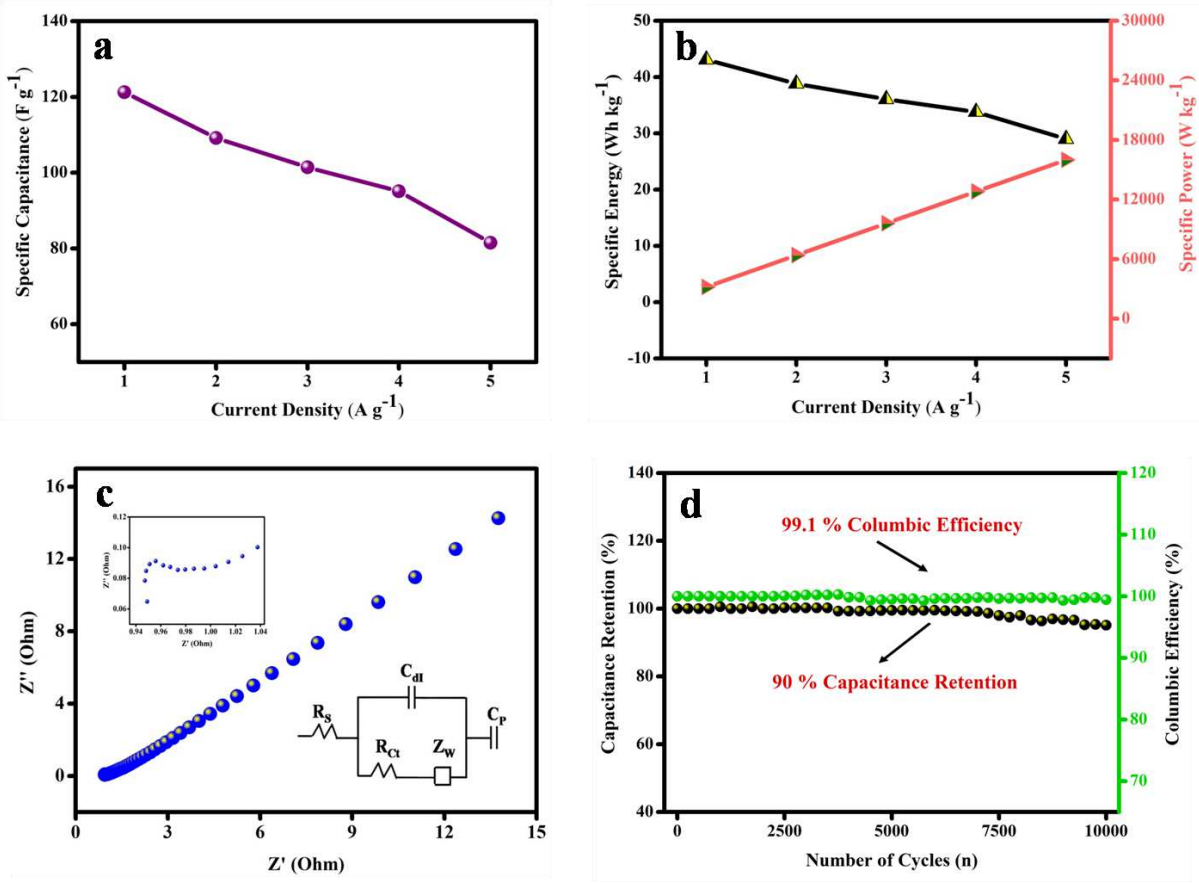


Figure. 7 (a) Specific capacitance Vs current density for Ni-Gd@BTC MOF//AC(b) Plot of Specific Energy and Specific Power as a function of current density for Ni-Gd@BTC MOF//AC;(c) cycling stability of the Ni-Gd@BTC MOF//AC cell ;(d) EIS spectrum of cell (inserted equivalent circuit)

4. Conclusion

In summary, we have developed a simple and convenient hydrothermal route to synthesize a highly efficient Ni-Gd@BTC MOF electrode material for energy-storage applications. The morphological analyses clearly confirmed the successful formation of the Ni-Gd@BTC MOF with a uniform structure beneficial for charge storage. Electrochemical studies in a three-electrode configuration revealed that the as-prepared Ni-Gd@BTC MOF delivers excellent specific capacitance as well as remarkable cyclic stability, indicating its suitability as a high-performance electrode material. To evaluate its practical application, we

assembled the material into a two-electrode system. Consequently, we fabricated a battery-type asymmetric supercapacitor device (Ni-Gd@BTC MOF//AC). This device shows an impressive energy density of 43.11 Wh kg^{-1} and a power density of 3200 W kg^{-1} at a current density of 1 A g^{-1}. Furthermore, it maintains 90% capacitance retention even after 10,000 charge–discharge cycles at 5 A g^{-1}, demonstrating excellent long-term durability.This study reveals s that the synthesized Ni-Gd@BTC MOF is a highly promising candidate for next-generation supercapacitor applications due to its superior electrochemical properties and stable structural performance.

5. Funding

This research work was funded by DST SERB project no. EEQ/2022/000405/03, February, 2023 and supported by PSG College of Arts and Science, Coimbatore. The authors gratefully acknowledge financial assistance from the DST SERB.

This research was funded by the University of Idaho Faculty Startup Grant, College of Engineering (Index No. 831707). The authors gratefully acknowledge the financial support provided by the University of Idaho.

6. Data Availability

The data's analyzed during the current study available from the corresponding author on reasonable request and all data generated during this study are included in this published article.

7. References

[1] A.G. Olabi, Q. Abbas, A. Al Makky, M.A. Abdelkareem, Supercapacitors as next generation energy storage devices: Properties and applications, Energy 248 (2022) 123617. https://doi.org/10.1016/j.energy.2022.123617.

[2] H.D. Yoo, E. Markevich, G. Salitra, D. Sharon, D. Aurbach, On the challenge of developing advanced technologies for electrochemical energy storage and conversion, Materials Today 17 (2014) 110–121. https://doi.org/10.1016/j.mattod.2014.02.014.

[3] Y. Ma, X. Xie, W. Yang, Z. Yu, X. Sun, Y. Zhang, X. Yang, H. Kimura, C. Hou, Z. Guo, W. Du, Recent advances in transition metal oxides with different dimensions as electrodes for high-performance supercapacitors, Adv Compos Hybrid Mater 4 (2021) 906–924. https://doi.org/10.1007/s42114-021-00358-2.

[4] S. Sagadevan, A.R. Marlinda, Z.Z. Chowdhury, Y.B.A. Wahab, N.A. Hamizi, M.M. Shahid, F. Mohammad, J. Podder, M.R. Johan, Fundamental electrochemical energy storage systems, in: Advances in Supercapacitor and Supercapattery, Elsevier, 2021: pp. 27–43. https://doi.org/10.1016/B978-0-12-819897-1.00001-X.

[5] W.J. Basirun, I.M. Saeed, M.S. Rahman, S.A. Mazari, Nickel oxides/hydroxides-graphene as hybrid supercapattery nanocomposites for advanced charge storage materials – a review, Critical Reviews in Solid State and Materials Sciences 46 (2021) 553–586. https://doi.org/10.1080/10408436.2021.1886040.

[6] Y. Peng, J. Xu, J. Xu, J. Ma, Y. Bai, S. Cao, S. Zhang, H. Pang, Metal-organic framework (MOF) composites as promising materials for energy storage applications, Advances in Colloid and Interface Science 307 (2022) 102732. https://doi.org/10.1016/j.cis.2022.102732.

[7] S. Sundriyal, H. Kaur, S.K. Bhardwaj, S. Mishra, K.-H. Kim, A. Deep, Metal-organic frameworks and their composites as efficient electrodes for supercapacitor applications,

Coordination Chemistry Reviews 369 (2018) 15–38. https://doi.org/10.1016/j.ccr.2018.04.018.

[8] X. Yang, Y. Tian, S. Li, Y.-P. Wu, Q. Zhang, D.-S. Li, S. Zhang, Heterogeneous Ni-MOF/V_2 CT_x –MXene hierarchically-porous nanorods for robust and high energy density hybrid supercapacitors, J. Mater. Chem. A 10 (2022) 12225–12234. https://doi.org/10.1039/D2TA02114E.

[9] L. Yue, X. Wang, T. Sun, H. Liu, Q. Li, N. Wu, H. Guo, W. Yang, Ni-MOF coating MoS2 structures by hydrothermal intercalation as high-performance electrodes for asymmetric supercapacitors, Chemical Engineering Journal 375 (2019) 121959. https://doi.org/10.1016/j.cej.2019.121959.

[10] Y. Chen, D. Ni, X. Yang, C. Liu, J. Yin, K. Cai, Microwave-assisted synthesis of honeycomblike hierarchical spherical Zn-doped Ni-MOF as a high-performance battery-type supercapacitor electrode material, Electrochimica Acta 278 (2018) 114–123. https://doi.org/10.1016/j.electacta.2018.05.024.

[11] Q. Li, H. Guo, R. Xue, M. Wang, M. Xu, W. Yang, J. Zhang, W. Yang, Self-assembled Mo doped Ni-MOF nanosheets based electrode material for high performance battery-supercapacitor hybrid device, International Journal of Hydrogen Energy 45 (2020) 20820–20831. https://doi.org/10.1016/j.ijhydene.2020.05.143.

[12] M.M. Gul, K.S. Ahmad, A.G. Thomas, S. Alarifi, Supercapacitor with highly efficient rare earth metal conjugated transition metal chalcogenide photoactive electrode In:SnO2/Nd2S3:Ni9S8:Co9S8, Materials Science and Engineering: B 294 (2023) 116544. https://doi.org/10.1016/j.mseb.2023.116544.

[13] Q. Hu, B. Yue, H. Shao, F. Yang, J. Wang, Y. Wang, J. Liu, Facile syntheses of perovskite type LaMO3 (M=Fe, Co, Ni) nanofibers for high performance supercapacitor

electrodes and lithium-ion battery anodes, Journal of Alloys and Compounds 852 (2021) 157002. https://doi.org/10.1016/j.jallcom.2020.157002.

[14] D.L. Singh, T.K. Ghosh, V. Mishra, S. Ramasamy, M.K. Sahoo, R.R. Gangavarapu, Three-Dimensional Lanthanide-Based Nanoporous Metal–Organic Frameworks for High-Performance Supercapacitors, ACS Appl. Nano Mater. 5 (2022) 15237–15249. https://doi.org/10.1021/acsanm.2c03347.

[15] W. Liu, Y. Peng, H. He, W. Tan, Y. Chen, X. Dai, A novel Ni–La-Nd-Y flim on Ni foam to enhance hydrogen evolution reaction in alkaline media, International Journal of Hydrogen Energy 47 (2022) 10289–10297. https://doi.org/10.1016/j.ijhydene.2022.01.123.

[16] L. Feng, Y. Zhu, H. Ding, C. Ni, Recent progress in nickel based materials for high performance pseudocapacitor electrodes, Journal of Power Sources 267 (2014) 430–444. https://doi.org/10.1016/j.jpowsour.2014.05.092.

[17] S. Khokhar, P. Chand, H. Anand, Recent advancements in Ni-MOF template derived electrode materials for supercapacitor application: A mini review, Results in Chemistry 7 (2024) 101298. https://doi.org/10.1016/j.rechem.2023.101298.

[18] N. Manyani, P. Siwatch, S. Rana, K. Sharma, S.K. Tripathi, Study of electrochemical behaviour of binder-free nickel metal-organic framework derived by benzene-1,3,5-tricarboxylic acid for supercapacitor electrode, Materials Research Bulletin 165 (2023) 112320. https://doi.org/10.1016/j.materresbull.2023.112320.

[19] G. Boopathi, G.G. Karthikeyan, S.M. Jaimohan, A. Pandurangan, Dopant Effects of Gd3+ on the Electrochemical Pseudocapacitive Characteristics of Electroactive Mesoporous NiO Electrodes for Supercapacitors, (n.d.).

[20] H.H. El-Maghrabi, A.A. Nada, M.F. Bekheet, S. Roualdes, W. Riedel, I. Iatsunskyi, E. Coy, A. Gurlo, M. Bechelany, Coaxial nanofibers of nickel/gadolinium oxide/nickel

oxide as highly effective electrocatalysts for hydrogen evolution reaction, Journal of Colloid and Interface Science 587 (2021) 457–466. https://doi.org/10.1016/j.jcis.2020.11.103.

[21] R. Bhosale, S. Bhosale, P. Kumbhar, D. Narale, R. Ghaware, C. Jambhale, S. Kolekar, Design and development of a porous nanorod-based nickel-metal–organic framework (Ni-MOF) for high-performance supercapacitor application, New J. Chem. 47 (2023) 6749–6758. https://doi.org/10.1039/D3NJ00456B.

[22] T. Chen, T. Shen, Y. Wang, Z. Yu, W. Zhang, Y. Zhang, Z. Ouyang, Q. Cai, Y. Ji, S. Wang, In Situ Synthesis of Ni-BTC Metal–Organic Framework@Graphene Oxide Composites for High-Performance Supercapacitor Electrodes, ACS Omega 8 (2023) 10888–10898. https://doi.org/10.1021/acsomega.2c07187.

[23] H. Brunckova, E. Mudra, L. Rocha, E. Nassar, W. Nascimento, H. Kolev, A. Kovalcikova, Z. Molcanova, M. Podobova, L. Medvecky, Preparation and characterization of isostructural lanthanide Eu/Gd/Tb metal-organic framework thin films for luminescent applications, Applied Surface Science 542 (2021) 148731. https://doi.org/10.1016/j.apsusc.2020.148731.

[24] J. Sunil, C. Narayana, G. Kumari, K. Jayaramulu, Raman spectroscopy, an ideal tool for studying the physical properties and applications of metal–organic frameworks (MOFs), Chem. Soc. Rev. 52 (2023) 3397–3437. https://doi.org/10.1039/D2CS01004F.

[25] W. Yuan, K. Jiao, H. Yuan, H. Sun, E.G. Lim, I. Mitrovic, S. Duan, S. Cong, R. Yong, F. Li, P. Song, Metal–Organic Frameworks/Heterojunction Structures for Surface-Enhanced Raman Scattering with Enhanced Sensitivity and Tailorability, ACS Appl. Mater. Interfaces 16 (2024) 26374–26385. https://doi.org/10.1021/acsami.4c01588.

[26] S. Wang, J. Wang, M. Zeng, J. Yang, N. Hu, Y. Su, Z. Zhou, H. Pang, Z. Yang, Synthesis of nickel-metal organic framework nanoplates with pyridine modulation and

application to supercapacitors, Journal of Energy Storage 38 (2021) 102528. https://doi.org/10.1016/j.est.2021.102528.

[27] N. Jeromiyas, M. Govindasamy, A.A. Alothman, M. Ouladsmane, C.-H. Huang, Synthesis of Gadolinium-Doped Molybdenum Diselenide Nanospheres for Ultrasensitive Electrochemical Determination of Essential Amino Acid in Human Serum and Milk Samples, J. Electrochem. Soc. 170 (2023) 057501. https://doi.org/10.1149/1945-7111/acced1.

[28] Y. Han, J. Zhou, L. Wang, L. Xing, Z. Xue, Y. Jiao, Y. Pang, Redox-active nanostructure electrode of Mn/Ni bimetal organic frameworks anchoring on multi-walled carbon nanotubes for advanced supercapacitor, Journal of Electroanalytical Chemistry 882 (2021) 114993. https://doi.org/10.1016/j.jelechem.2021.114993.

[29] B. Chettiannan, S. Mathan, G. Arumugam, A. Srinivasan, R. Rajendran, Attaining high energy density using metal-organic framework-derived NiO/Co3O4/NiCo2O4 as an electrode in asymmetric hybrid supercapacitor, Journal of Energy Storage 77 (2024) 110008. https://doi.org/10.1016/j.est.2023.110008.

[30] Sonadia, W. Miran, Z. Iqbal, M. Shah, G. Mustafa, M.U. Mushtaq, A. Ul-Hamid, F. Azad, High-performance cauliflower-like Er2O3/NiO nanocomposite derived from Er-Ni-MOF for energy conversion and storage applications, Journal of Energy Storage 108 (2025) 115222. https://doi.org/10.1016/j.est.2024.115222.

[31] S. Gao, Y. Sui, F. Wei, J. Qi, Q. Meng, Y. Ren, Y. He, Dandelion-like nickel/cobalt metal-organic framework based electrode materials for high performance supercapacitors, Journal of Colloid and Interface Science 531 (2018) 83–90. https://doi.org/10.1016/j.jcis.2018.07.044.

[32] J.R. Durga, C. Rakkappan, Structural, Morphological and Electrochemical Properties of Gd doped Fe3O4 Nanoparticles for Supercapacitor Applications, Ajc 37 (2025) 2397–2405. https://doi.org/10.14233/ajchem.2025.34199.

[33] S. Sharif, M. Shahbaz, T.T. Rehman Afzal, M. Saeed, A. Shahzad, S. Shahzad, M.N. Asghar, S. Hussain, A. Bentalib, A.B. Jumah, Nitrogen-rich Gadolinium 2D cubic layered metal organic framework for high performance energy storage devices, Materials Chemistry and Physics 345 (2025) 131279. https://doi.org/10.1016/j.matchemphys.2025.131279.

[34] B. Chettiannan, G. Arumugam, S. Mathan, M. Selvaraj, M.A. Assiri, R. Rajendran, Exploring the effect of metal ratio on electrochemical properties of MOF-derived microporous flower-like NiO/Co3O4 electrodes for high-performance asymmetric supercapacitor application, Journal of Energy Storage 119 (2025) 116326. https://doi.org/10.1016/j.est.2025.116326.

[35] W. Lu, L. Yan, W. Ye, J. Ning, Y. Zhong, Y. Hu, Defect engineering of electrode materials towards superior reaction kinetics for high-performance supercapacitors, J. Mater. Chem. A 10 (2022) 15267–15296. https://doi.org/10.1039/D2TA02930H.

[36] X. Zhang, N. Qu, S. Yang, Q. Fan, D. Lei, A. Liu, X. Chen, Shape-controlled synthesis of Ni-based metal-organic frameworks with albizia flower-like spheres@nanosheets structure for high performance supercapacitors, Journal of Colloid and Interface Science 575 (2020) 347–355. https://doi.org/10.1016/j.jcis.2020.04.127.

[37] S. Yazdani, M.S. Lashkenari, F. Mehri, Design a novel mixed-ligand Ni-MOF/MWCNT nanocomposite to enhance the electrochemical performance of supercapacitors, Synthetic Metals 307 (2024) 117702. https://doi.org/10.1016/j.synthmet.2024.117702.

[38] B. Li, R. Zhao, H. Yue, Y. Zhang, S. Lu, W. Shang, Z. Zhang, Y. Wen, In situ electrodeposition construction of a Ni/Mn bimetallic organic framework material and its

electrochemical performance in flexible supercapacitors, Journal of Alloys and Compounds 1020 (2025) 179340. https://doi.org/10.1016/j.jallcom.2025.179340.

[39] M. Kashif, S. Thangarasu, N. Murugan, S.S. Magdum, Y.A. Kim, M. Kurkuri, T.-H. Oh, Interatomic interaction of 2D crumpled V2O5 nanosheets layered with Ni-MOF as a bifunctional electrocatalyst for overall water splitting and supercapacitor applications, Journal of Energy Storage 81 (2024) 110348. https://doi.org/10.1016/j.est.2023.110348.

[40] Y. Ding, Z. Yan, G. Wang, H. Sang, W. Li, Z. Xu, One-pot preparation of La-doped Ni-MOF nanospheres for efficient hybrid supercapacitor electrode material, Materials Chemistry and Physics 309 (2023) 128340. https://doi.org/10.1016/j.matchemphys.2023.128340.

[41] X. Sun, J. Chen, W. Kong, Q. Yu, C. Hu, Y. Long, Y. Dai, J. Gong, L. Pu, H. Zhang, W. Wang, Cr-doped Ni-MOF nanosheet array structure anchored on nickel foam with specific orientation for high performance supercapacitors, Electrochimica Acta 469 (2023) 143264. https://doi.org/10.1016/j.electacta.2023.143264.

[42] M.S. Rahmanifar, H. Hesari, A. Noori, M.Y. Masoomi, A. Morsali, M.F. Mousavi, A dual Ni/Co-MOF-reduced graphene oxide nanocomposite as a high performance supercapacitor electrode material, Electrochimica Acta 275 (2018) 76–86. https://doi.org/10.1016/j.electacta.2018.04.130.

[43] H. Duan, M. Shi, M. Zhang, G. Feng, S. Liu, C. Chen, Lanthanum Oxide Nickel Hydroxide Composite Triangle Nanosheets for Energy Density Asymmetric Supercapacitors, Front. Chem. 9 (2021) 783942. https://doi.org/10.3389/fchem.2021.783942.

[44] D. Jiang, C. Wei, Z. Zhu, X. Xu, M. Lu, G. Wang, Preparation of Flower-like Nickel-Based Bimetallic Organic Framework Electrodes for High-Efficiency Hybrid Supercapacitors, Crystals 11 (2021) 1425. https://doi.org/10.3390/cryst11111425.